Role of Boron in Amorphous-InGaZnO Film for Resistance Control Technique

Keisuke Yasuta[1], Toshimasa Ui[1], Tomokazu Nagao[1], Daisuke Matsuo[2], Toshihiko Sakai[2], Yoshitaka Setoguchi[2], Eiji Takahashi[2], Yasunori Andoh[2] and Junichi Tatemichi[1]

E-mail: ui_toshimasa@nissin.co.jp
[1] NISSIN ION EQUIPMENT CO., LTD.
29, Hinokigaoka, Minakuchi-cho, Koka, Shiga, 528-0068, Japan
[2] NISSIN ELECTRIC CO., LTD.
47, Umezu-Takase-cho, Ukyo-ku, Kyoto, 615-8686, Japan
Keywords: Boron, Implantation, IGZO, Resistance

ABSTRACT

As a next-generation electronics material, amorphous indium-gallium-zinc oxide (a-IGZO) film devices were investigated. In order to further utilize a-IGZO films, we carried out boron ion implantation and analyzed the implanted a-IGZO using Hall measurements with wet etching processes. As a result, we clarified that the implanted boron decreases a-IGZO resistance, which can be applied to drastically sheet resistance reduction methods for a-IGZO device processing.

1 Introduction

Amorphous indium-gallium-zinc oxide (a-IGZO) attracts much attention for next-generation flat-panel displays due to the large band gap, light transparency, printability and low-temperature in film deposition. Using a-IGZO films, thin-film-transistors (TFTs) are realized, which show superior behavior compared with amorphous Si-based TFT [1, 2]. In order to further improve a-IGZO TFT performance via source-drain resistance reduction, plasma treatment [3], excimer laser annealing [4] and ion implantation [5, 6] methods as the sheet resistance reduction techniques were investigated. Among them, the ion implantation methods have depth control ability through insulator layers and microfabrication ability owing to the small channel length reduction. In our previous work we elucidated that a-IGZO sheet resistance reduction can be attributed to oxygen vacancy (Vo) generated by noble gas implantation [7]. However, there is still much room for clarifying and improving the implantation method, since many injectable ion species in a-IGZO are not investigated in detail. In this work, we carried out one of the conventional ion B^+ implantation and investigation in a-IGZO thin film on glass. Electron transport properties of B^+ implanted a-IGZO films as a function of the a-IGZO depth were investigated by Hall measurements combined with wet etchings. In addition, Vo concentration profile in the a-IGZO is calculated by a simulation. On the other hand, bonding analysis by X-ray photoelectron spectroscopy (XPS) were carried out. As results, we clarified roles of boron in a-IGZO film for resistance control technique.

2 Experiments and results

We prepared a-IGZO films with a film thickness 50 nm and a sheet resistance ~ 10^{13} Ω/sq. deposited by inductively coupled plasma (ICP) sputtering on a glass (0.5-mm-thick EAGLE XG), in which conditions are gas flow Ar/O_2 = 95/5 sccm, pressure 0.9 Pa, RF power 7 kW and $InGaZnO_4$ target voltage −400 V [8]. In order to decrease the sheet resistance and fabricate implantation

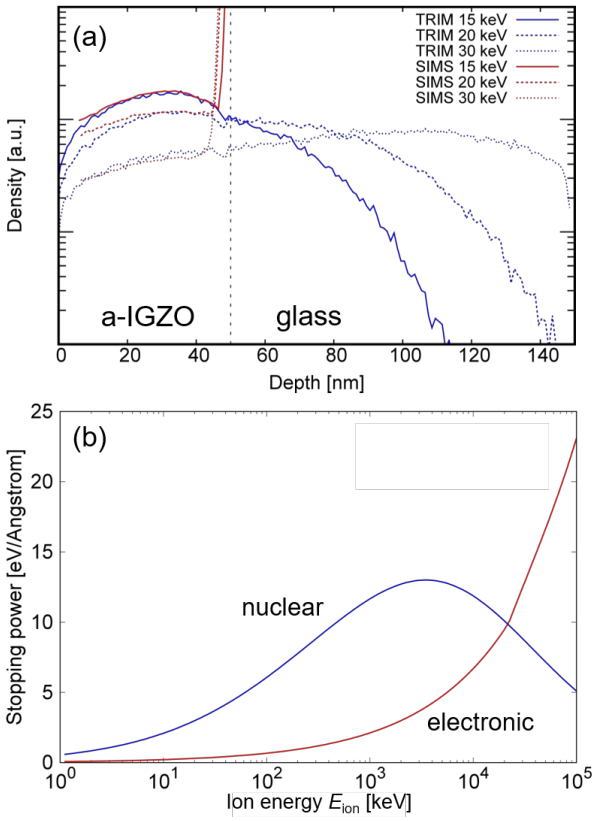

Fig. 1 (a) B depth profiles in a-IGZO (50 nm)/glass structure of each ion energy E_{ion} measured by secondary mass spectrometry (SIMS) and calculated by a simulator TRIM [10]. **(b)** electronic and nuclear stopping power as a function of B^+ energy in the a-IGZO obtained by the SIMS and the TRIM shown in Fig.1 (a).

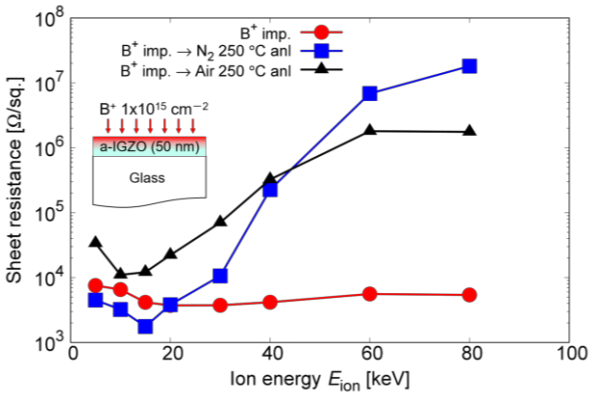

Fig. 2 Sheet resistances as functions of E_{ion} of 50-nm-thick a-IGZO films on glass with B^+ implantation (B^+ imp.) and with annealing process in N_2 ambient of 250 °C after B^+ implantation (B^+ imp. → N_2 250 ºC anl) or and with annealing process in air of 250 °C after B^+ implantation (B^+ imp. → Air 250 ºC anl), respectively, where dose amounts are 1×10^{15} cm^{-2}.

depth control technique, B^+ ion implantations with the ion energy range of 15-30 keV in the a-IGZO/glass structure were carried out using ion implanter iG series [9] and the implantation depth profiles were measured by secondary mass spectrometry (SIMS) as shown in Fig. 1 (a). From B depth profile in the a-IGZO, we estimated electronic and nuclear stopping power as a function of ion energy E_{ion} of B^+ in the a-IGZO calculated by a simulator (Transport or Ions in Matter TRIM) [10] as shown in Fig.1 (b). Hence, we fabricated B^+ implantation depth control technique. On the other hand, we carried out B^+ implantation in the a-IGZO films for the purpose of implantation ion energy optimazation, where the E_{ion} ranges are 5-80 keV with uniform dose 1×10^{15} cm^{-2}, respectively . In addition, post-annealing (anl) in N_2 ambient or the air at 250 ºC 1 hour were carried out. From Hall measurement, we obtained the a-IGZO sheet resistance as a function of the E_{ion} as shown in Fig. 2. Although B^+ implanted a-IGZO sheet resistance decreases with increasing E_{ion} of 10-20 keV, a-IGZO sheet resistance increases with increasing in the range of 20-80 keV, which behaviors almost corresponds to B amounts in a-IGZO films as shown in Fig. 1 (a). In addition, we find that the increase or decrease behaviors are emphasized after the annealing processes. In addition, the annealed a-IGZO films in the air ambient exhibit resistance increase comparison with the N_2 annealed sample, since oxidizer H_2O and O_2 in the air reduce Vo in a-IGZO films. In order to analyze the sheet resistance reduction, XPS analyses of B^+ implanted a-IGZO films were carried out. Figure 3 (a) shows XPS global spectra for a-IGZO without implantation and with B^+ 15 keV, 1×10^{15} cm^{-2} implantation and with the N_2 annealing process after the implantation, where the binding energies were calibrated to common C1s peak at 284.6 eV. Figure 3 (b) shows XPS B1s spectra for a-IGZO without implantation and with the implantation and with the annealing process after the implantation. Considering B1s binding energy 188 eV [11] for B-B bonding and electron negativity relationship of Zn (1.65) < In (1.78) < Ga (1.81) < B (2.04) < O (3.44), we find that B-O bonding effect is dominant for the implanted boron. On the other hand, we previously reported that O1s spectra exhibit Vo decreases after the annealing [12]. Hence, we find a possibility that a-IGZO sheet resistance reduction can be realized by not only Vo but also the boron itself. In order to separate between the boron and the Vo effects in a-IGZO, we carried out the B^+ 50 keV with 1×10^{15} cm^{-2} implantation in 180-nm-thick a-IGZO film. In addition, we carried out depth profile analyses using Hall measurement combined with wet etching. From Hall measurements, as shown in Fig. 4 (a), (b) and (c), we obtained sheet resistances, Hall mobilities μ_{meas} and sheet concentration n_{meas} as a function of the etching

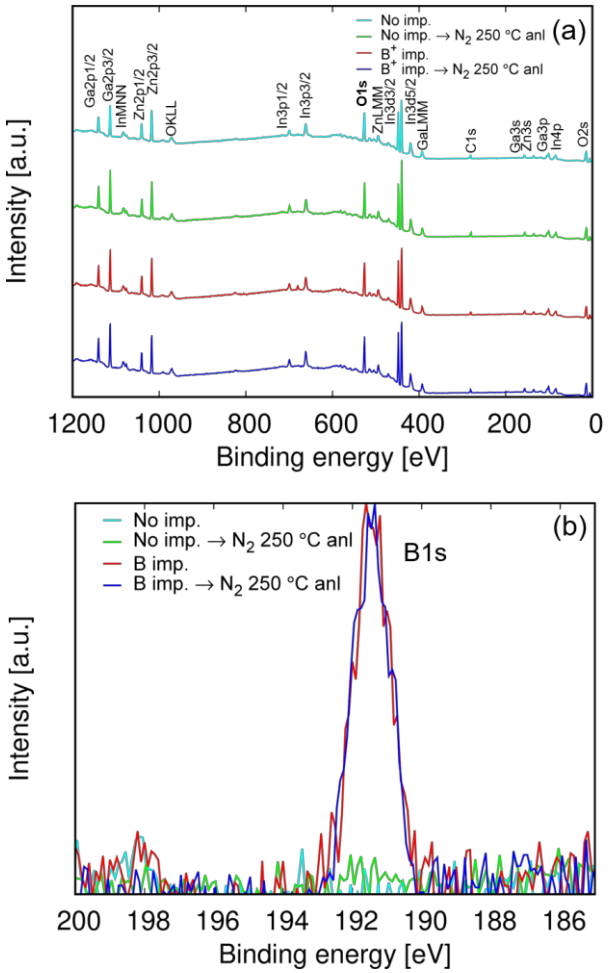

Fig. 3 (a) X-ray photoelectron spectroscopy (XPS) global spectra for 50-nm-thick a-IGZO films without implantation and with B^+ 15 keV, 1×10^{15} cm^{-2} implantation and with the annealing process in N_2 ambient after the implantation. **(b)** XPS B1s spectra for 50-nm-thick a-IGZO films without implantation and with the B^+ implantation and with the annealing process after the implantation.

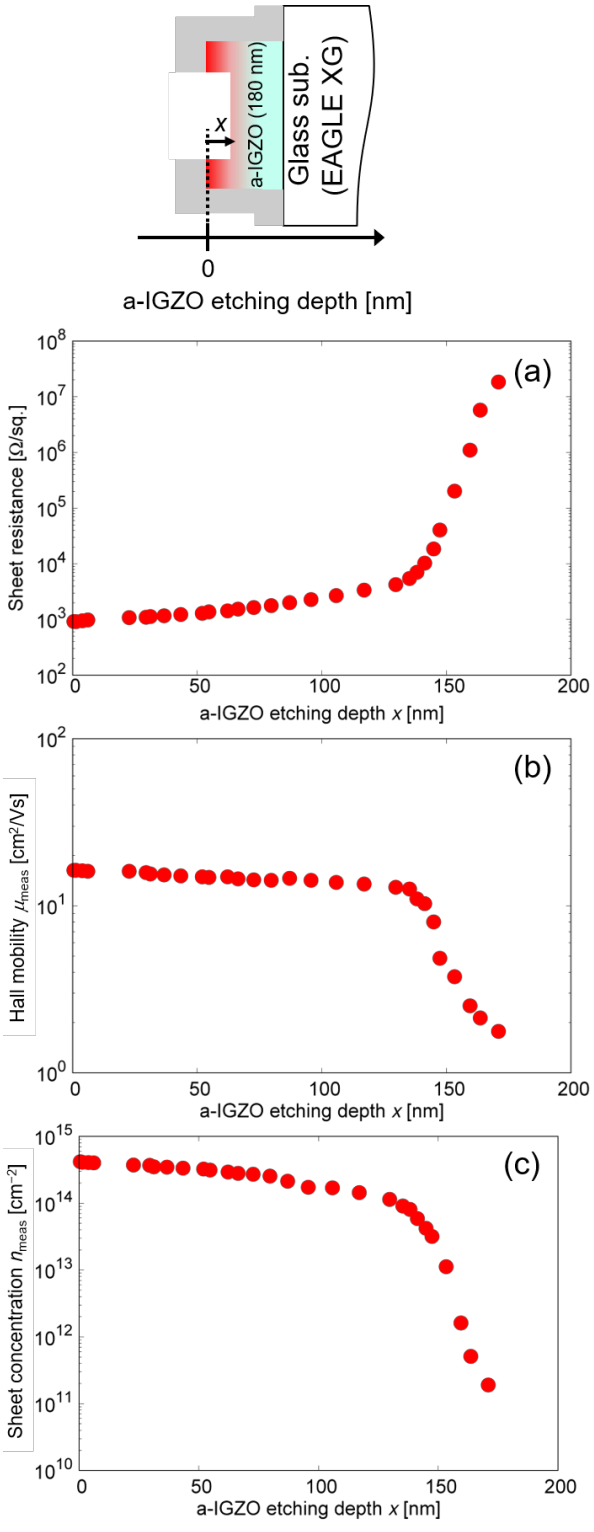

Fig. 4 (a) Sheet resistance, **(b)** Hall mobilities and **(c)** sheet concentrations as a function of B^+ implanted 180-nm-thick a-IGZO etching depth x from the a-IGZO surface before the etching processes, where the implantation condition is ion energy 50 keV and dose 1 $\times 10^{15}$ cm^{-2}, respectively.

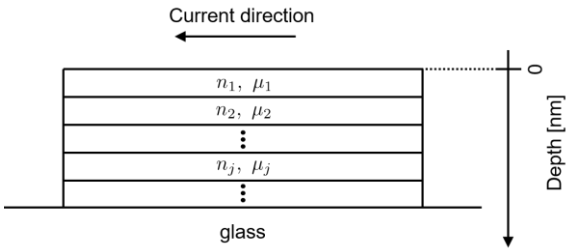

Fig. 5 Local electron concentration n_j and local electron mobility μ_j model of the a-IGZO.

depth x from the a-IGZO surface. The sheet resistance slowly increases with increasing in x < 150 nm. In addition, both μ_{meas} and n_{meas} slowly decrease with increasing in x < 150 nm also, which indicates B^+ penetration ability and resistance reduction ability are higher than that of Ar^+ reported previously [12]. In order to estimate the local electron concentration n_j and local Hall mobility μ_j profiles as functions of a-IGZO depth, we considered a parallel conductance model in the a-IGZO film shown in Fig. 5. In case of the electrical transport properties development in each etching layer and a weak-magnetic-field ($\mu_{meas}B$ << 1, where μ_{meas} = 1-20 cm^2/Vs as shown in the Fig. 4 and the magnetic flux density B ~ 0.5 Tesla) approximation applicable, two independent equations consist as follows:

$$\sigma_{\mathrm{meas}}(x) = n_{\mathrm{meas}}(x) \cdot \mu_{\mathrm{meas}}(x),\ \ \sigma_j = n_j \cdot \mu_j,$$

$$\sigma_{\mathrm{meas}}(x) \simeq \sum \sigma_j, \qquad (1)$$

$$\sigma_{\mathrm{meas}}(x) \cdot \mu_{\mathrm{meas}}(x) \simeq \sum \sigma_j \mu_j^2, \qquad (2)$$

where the σ_{meas}, n_{meas}, and μ_{meas} are conductance, electron concentration and Hall mobility obtained by the Hall measurements as shown in Fig. 4, respectively. Hence, n_j and μ_j as functions of a-IGZO depth can be estimated by the simultaneous equation (1) and (2). Figure 6 (a) and (b) shows concentrations and local Hall mobilities as functions of a-IGZO depth, where the depth zero corresponds to the a-IGZO surface. In addition, we estimated boron and Vo concentration profiles as shown in Fig. 6 (a), where the boron and Vo profiles are calculated by TRIM using the electronic and nuclear stopping powers for B in a-IGZO as shown in Fig.1 (b) and the bonding energies of In, Ga, Zn and O are ~ 3 eV [13], respectively. From comparison between the n_j and Vo and B concentrations, the Vo concentration profile is not agreement with n_l profile only, but also agreement the B profiles at the deep position around 150 nm of a-IGZO. On the other hand, μ_j profile also almost uniform value in the a-IGZO deep position, which indicates also that boron itself contribute the a-IGZO resistance reduction. We find that the Hall measurement with the wet etching results are good agreement with the Hall measurement of each ion energy combined the SIMS results and the XPS results.

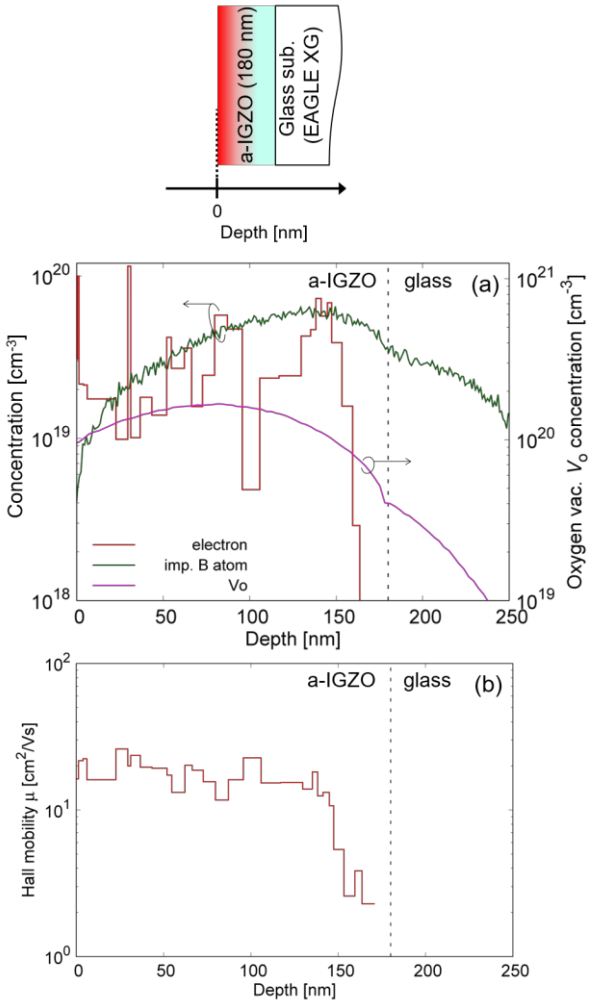

Fig. 6 (a) Concentrations and **(b)** local electron mobilities as functions of a-IGZO depth, where the depth zero corresponds to the a-IGZO surface.

3 Summary

We investigated B^+ implantation 50-nm-thick a-IGZO films on the glass, in which a-IGZO films were prepared by ICP sputtering system. On the other hand, the B^+ implantations were carried out by using iG series. From Hall measurement, B^+ implanted a-IGZO sheet resistances have bottom value in the range of 10-80 keV, which behaviors corresponds to B amounts in a-IGZO films, from which we obtained one of the minimum sheet resistance realized by optimized E_{Ion}. From the SIMS results and the XPS results and Hall measurements combined wet etching processes, we find a role of implanted boron in a-IGZO, which exhibits a-IGZO sheet resistance reduction can be realized by implanted boron itself. We expect that the B^+ implantation technology for a-IGZO sheet resistance control technique is much useful for a-IGZO device processing.

References

[1] K. Nomura, H. Ohta, A. Takagi, T. Kamiya, M. Hirano and H. Hosono, "Room-Temperature Fabrication of Transparent Flexible Thin-Film Transistors Using Amorphous Oxide Semiconductors" Nature **432** (2004) 488.

[2] T. Kamiya, K. Nomura and H. Hosono, "Origins of High Mobility and Low Operation Voltage of Amorphous Oxide TFTs: Electronic Structure, Electron Transport, Defects and Doping" J. Disp. Technol. **5** (2009) 273.

[3] H. Jeong, B. Lee, Y. Lee, J. Lee, M. Yang, I. Kang, M. Mativenga and J. Jang, "Coplanar amorphous-indium-gallium-zinc-oxide thin film transistor with He plasma treated heavily doped layer" Appl. Phys. Lett. **104** (2014) 022115.

[4] M. Nakata, H. Tsuji, Y. Fujisaki, H. Sato, Y. Nakajima, T. Takei, T. Yamamoto and T. Kurita, "Fabrication method for self-aligned bottom-gate oxide thin-film transistors by utilizing backside excimer-laser irradiation through substrate" Appl. Phys. Lett. **103** (2013) 142111.

[5] R. Chowdhurya, M. Kabirb, R. Manleyc and K. Hirschman, "Self-Aligned IGZO TFTs with Boron Implanted Source/Drain Regions" ECS Transactions **92** (2019) 135.

[6] L. Qian, W. Tang and P. Laia, "Improved Characteristics of InGaZnO Thin-Film Transistor by Using Fluorine Implant" ECS Solid State Lett. **3** (2014) 87.

[7] T. Ui, R. Fujimoto, T. Sakai, D. Matsuo, Y. Setoguchi, Y. Andoh and J. Tatemichi, "Characteristics of noble-gas-ion-implanted amorphous-InGaZnO films on glass" **27th** AM-FPD '20 (2020) 115.

[8] D. Matsuo, R. Miyanaga, T. Ikeda, S. Kishida, Y. Setoguchi, Y. Andoh, M. N. Fujii and Y. Uraoka, "Deposition of Crystalline InGaZnO Film at Low Temperature Process by Inductively Coupled Plasma Sputtering System" the **25th** IDW '18, FMCp7-2L (2018) 560.

[9] S. Dohi, H. Kai, T. Nagao, T. Matsumoto, M. Onoda, K Nakao, Y. Inouchi, J. Tatemichi and M. Nukayama, The Nissin Electric Review **62** (2017) 17.

[10] J. Ziegler and J. Biersack, Stopping Power and Range of Ion in Matter (2008).

[11] A. Thompson, and D. Vaughan, X-RAY DATA BOOKLET (2009).

[12] T. Ui, R. Fujimoto1, K. Yasuta, D. Matsuo, T. Sakai, Y. Setoguchi, E. Takahashi, Y. Andoh and J. Tatemichi, the **27th** IDW '20, FMCp3-5 (2020) 315.

[13] K. Takechi, Y. Kuwahara, J. Tanaka and H. Tanabe, "Depth-profiling XPS analysis of He-plasma treated amorphous InGaZnO thin films for use in top-gate coplanar thin-film transistors" Jpn. J. Appl. Phys. **58** (2019) 038005.